



Supplement of

Exploring the use of multi-source high-resolution satellite data for snow water equivalent reconstruction over mountainous catchments

Valentina Premier et al.

Correspondence to: Valentina Premier (valentina.premier@eurac.edu)

The copyright of individual parts of the supplement might differ from the article licence.

S1 In-situ snow measurements

State characterization is performed by observing available SWE or SD in-situ measurements. For the SFSJR, SWE continuous measurements are available for 7 different sites. As shown in Fig. 3a in the main text, only one station is within the considered area, i.e., the Volcanic Knob station (VLC). For this station, SWE records are available starting from 2000. This allowed us to perform an analysis of the SWE regime. In Fig. S1, we show the average SWE for all recorded years, the range of variation, and the current SWE. It is possible to see that the first season presents high SWE, while the other two seasons are under the average regime, especially the last one. For the SWE reconstruction, we also considered the stations in the surrounding area to smooth out possible sensor errors or redistribution effects.

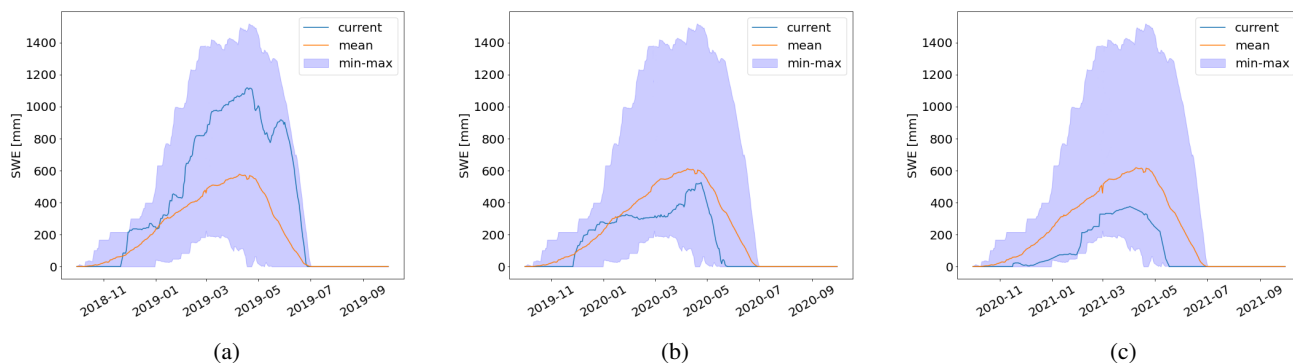


Figure S1. Average SWE (in orange) against the current SWE (in blue) and the range min-max SWE (in violet) at the Volcanic Knob test site for the hydrological seasons a) 2018/19, b) 2019/20 and c) 2020/21. SWE records are available starting from 2000.

In the Schnals catchment, SWE continuous records are available only for the location Bella Vista. For this reason, the decision on the state is based on the SD records available for 5 stations (see Fig. 3b in the main text). Three stations are within the study area and the remaining two are very close to the study area (maximum 5 km).

S2 Degree-day estimation

The DD is estimated from available in-situ temperature observations for both catchments. Regarding SFSJ, the temperature is available at 11 different stations located within a radius of approximately 15 km from the study area (see Fig. 3a). Due to the presence of some gaps in the data, we excluded from the computation of the DD the station "RKC" for season 2018/19, "WWC" for 2019/20 and "DKY", "VLC", and "UBC" for 2020/21. For the Schnals catchment, the temperature is available in 15 different locations within a maximum distance of around 10 km (see Fig. 3b). Once the DD is computed for each station through Eq. 2, the DD is spatially interpolated with the kriging routine as explained in Sec. 2.3. The goodness of the spatial interpolation is tested through a leave one out (LOO) cross-validation. The results in terms of root mean square error (RMSE) are reported in Fig. S2 for SFSJR and in Fig. S3 for Schnals, showing a mean RMSE that never exceeds $1.5^{\circ}\text{C}\cdot\text{d}$.

S3 SWE results for the South Fork of the San Joaquin River

Fig. S4 shows the SWE maps derived with the proposed method, the ASO reference maps, the bias calculated as the difference between the proposed and the reference maps and the dispersion graphs for the 12 analyzed dates over three hydrological seasons (2018-2021) for the SFSJR. The maps have a spatial resolution of 50 m. The scatterplots suggest a dispersion, even though most of the points are generally concentrated on the diagonal.

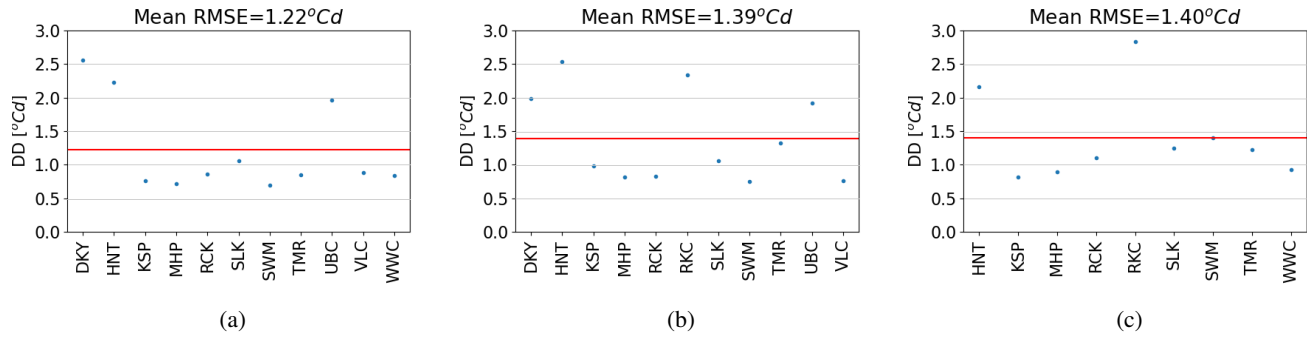


Figure S2. Leave-one-out cross validation results for the SFSJR for the hydrological seasons a) 2018/19, b) 2019/20 and c) 2020/21.

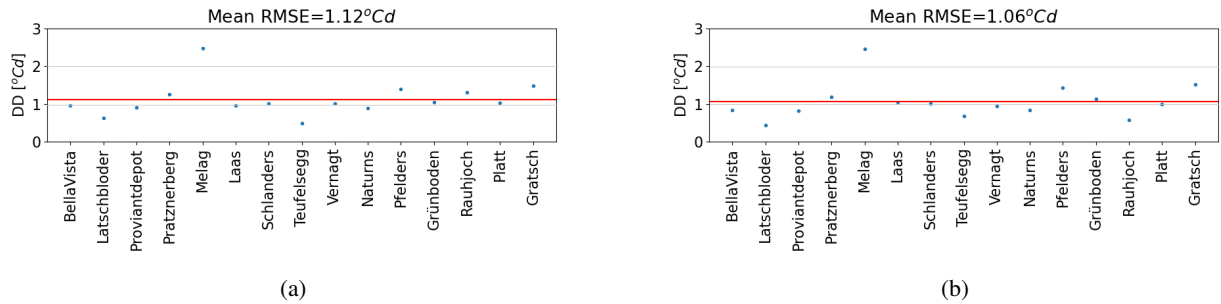
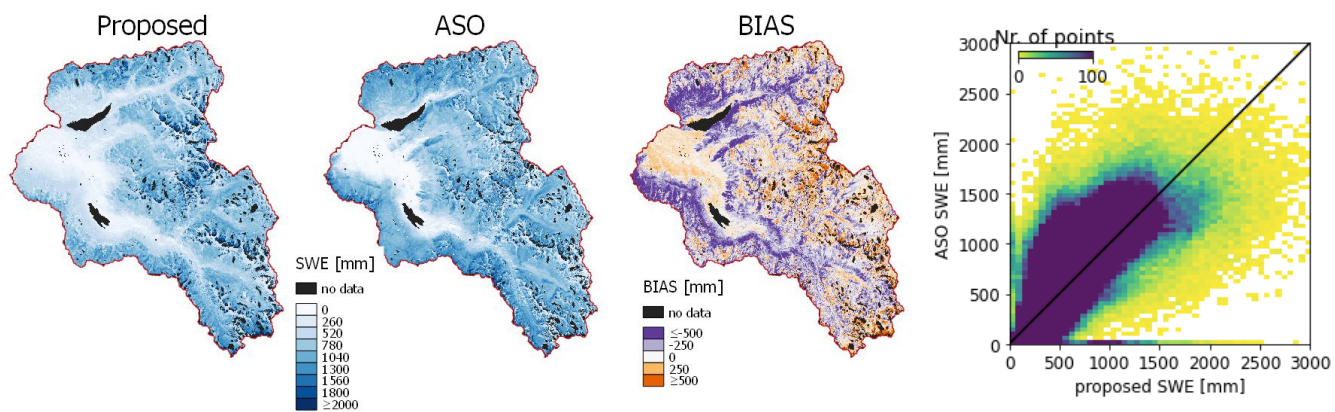


Figure S3. Leave-one-out cross validation results for the Schnals catchment for the hydrological seasons a) 2019/20 and b) 2020/21).

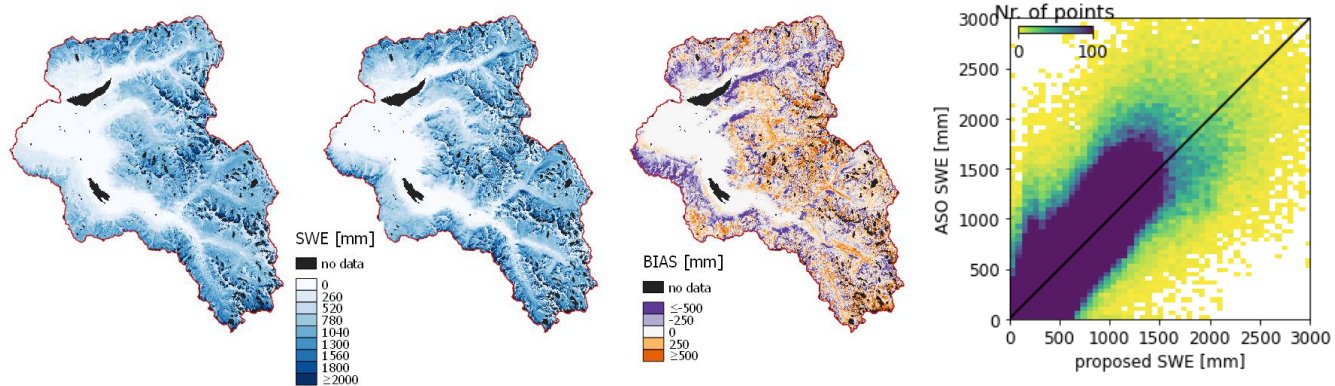
Similarly, Fig. S5 shows the SWE maps derived with the proposed method, the ASO SWE maps, the WUS-SR SWE maps, and the dispersion graphs between the proposed and the WUS-SR SWE for the same 12 analyzed dates over three hydrological seasons (2018-2021) for the SFSJR. The maps have a spatial resolution of 500 m.

Fig. S6 shows the mean SWE calculated for different elevation, slope and aspect bands for the 12 dates when also the ASO reference is available. The analysis is carried out for the proposed method and ASO only, as the high spatial resolution allows for a better appreciation of the complex topographical variability. We can notice a general good agreement showing that the proposed method is able to represent the typical topographical variability of the snow processes. The two datasets show similar trends when compared for different elevation belts. In general, a tendency of the proposed maps to underestimate SWE for lower elevations can be observed, while overestimating SWE for higher elevations. The slope analysis shows larger differences, especially for some dates (i.e., 9 June 2019 and the three images acquired for year 2020) and when considering steep slopes. The proposed method underestimates SWE w.r.t. ASO. However, we generally expect lower SWE for these steeper slopes that promote gravitational transport. The aspect analysis suggests an underestimation for the north facing slope when comparing our dataset with ASO (except for year 2021).

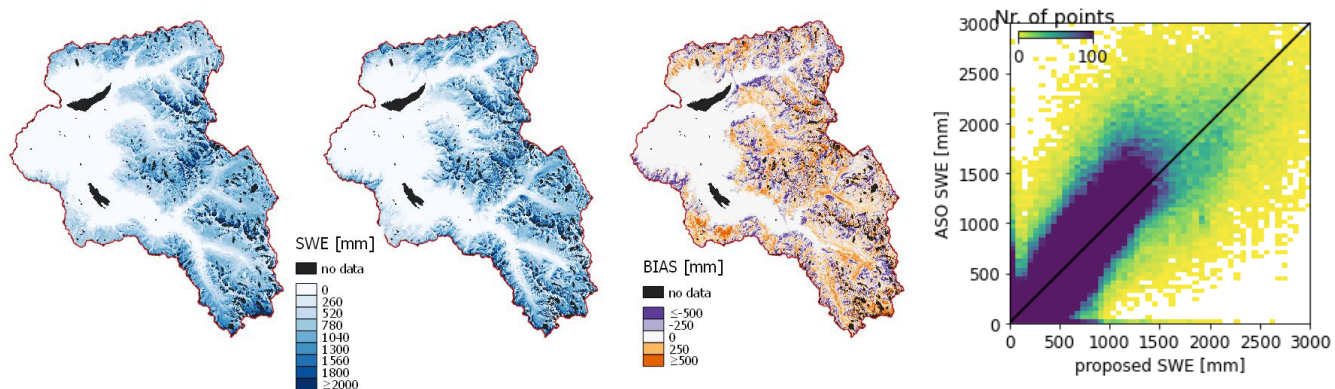
In conclusion, we also present in Table S1 the results of the intercomparison between the proposed SWE and the WUS-SR dataset versus ASO for the SFSJR. Bias, RMSE, and correlation are calculated pixel-wise. To this purpose, the proposed and ASO maps were aggregated at a resolution of 500 m. It is possible to notice that the proposed SWE presents a higher bias (an average of -34 mm versus 16 mm), while the RMSE is lower (151 mm versus 193 mm) and the correlation is higher (0.83 versus 0.65).



(a) 17 March 2019.

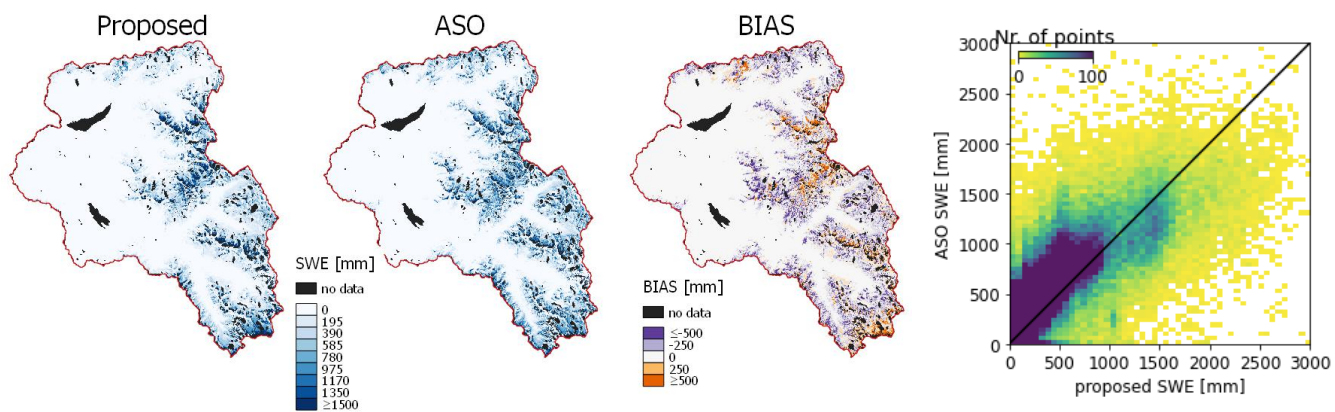


(b) 2 May 2019.

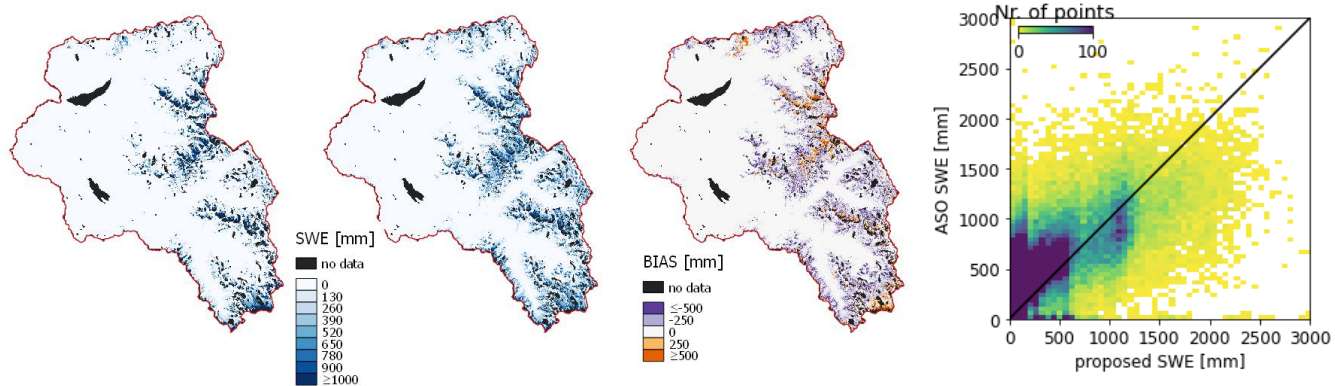


(c) 9 June 2019.

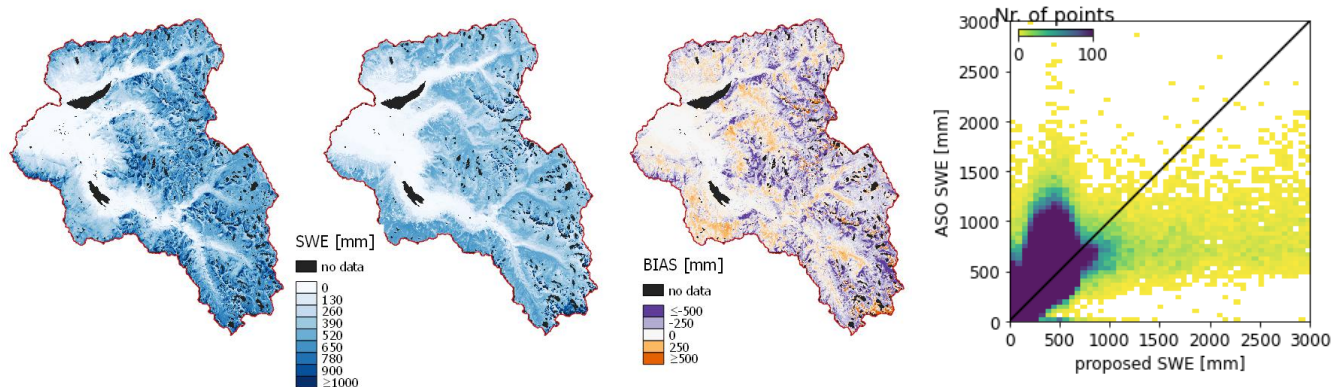
Figure S4. Proposed SWE (left), ASO SWE (centre-left), bias (centre-right) and dispersion graph (right) for the 12 analyzed dates over the three hydrological seasons (2018-2021) for the SFSJR.



(d) 4 July 2019.

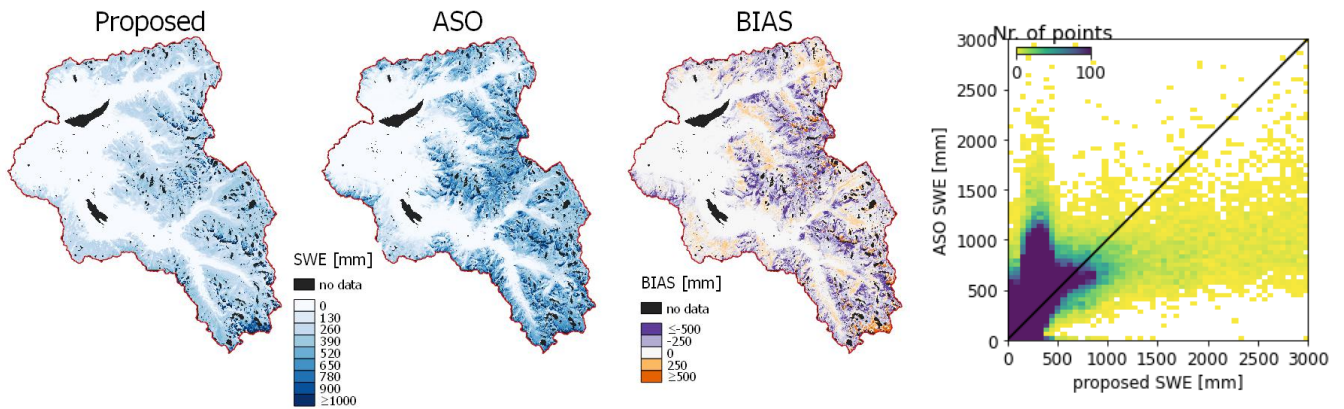


(e) 14 July 2019.

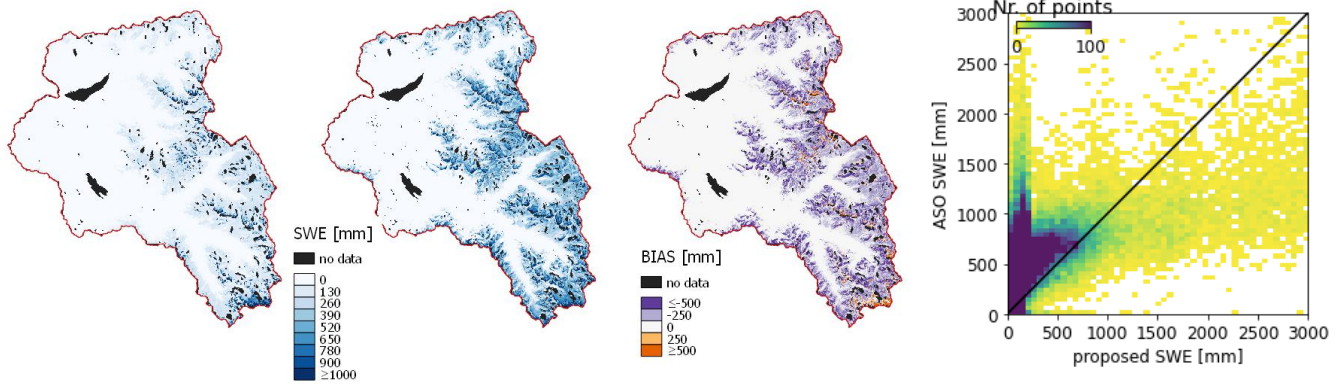


(f) 15 April 2020.

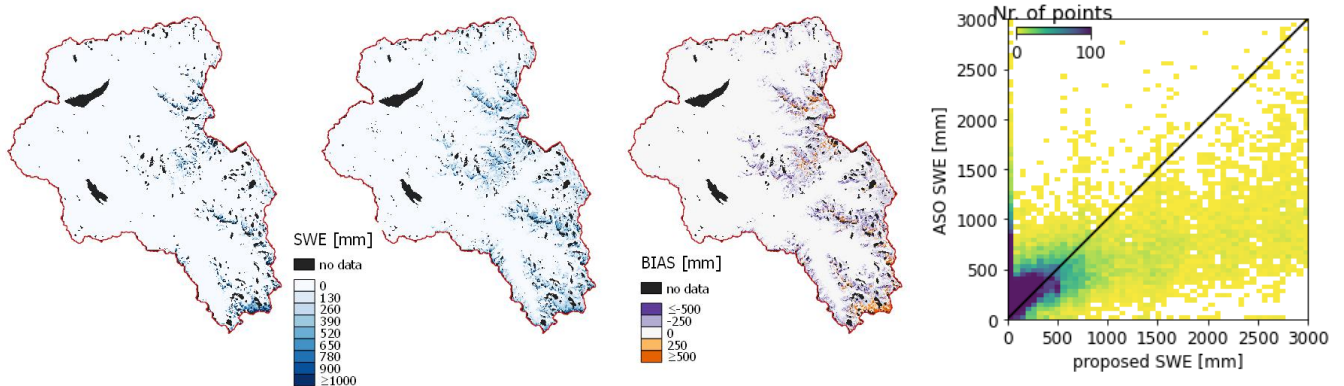
Figure S4. Proposed SWE (left), ASO SWE (centre-left), bias (centre-right) and dispersion graph (right) for the 12 analyzed dates over the three hydrological seasons (2018-2021) for the SFSJR. (cont.)



(g) 5 May 2020.

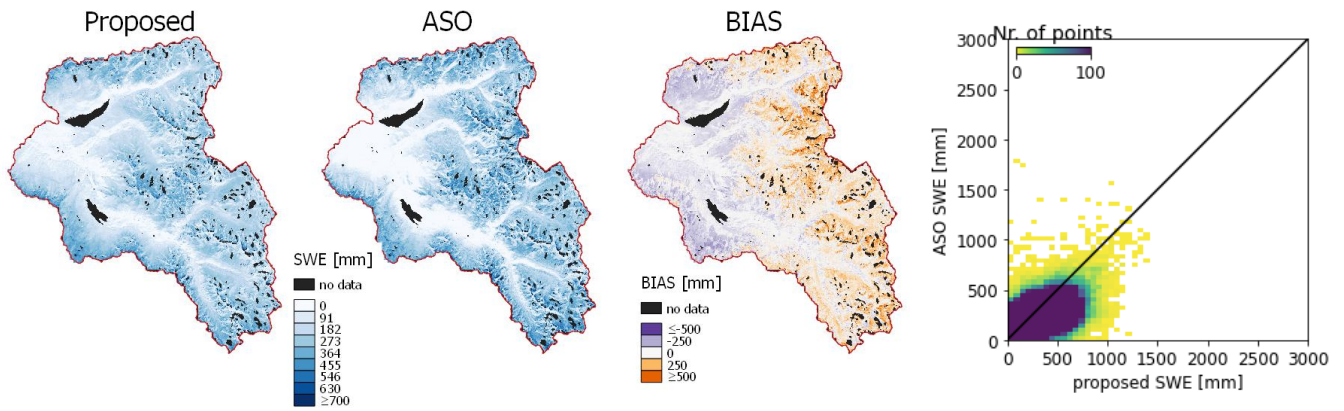


(h) 23 May 2020.

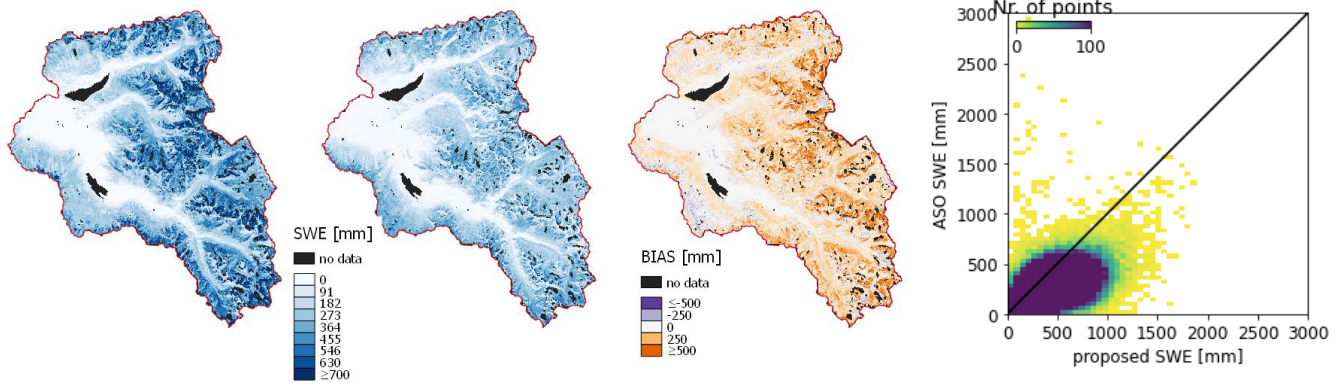


(i) 8 June 2020.

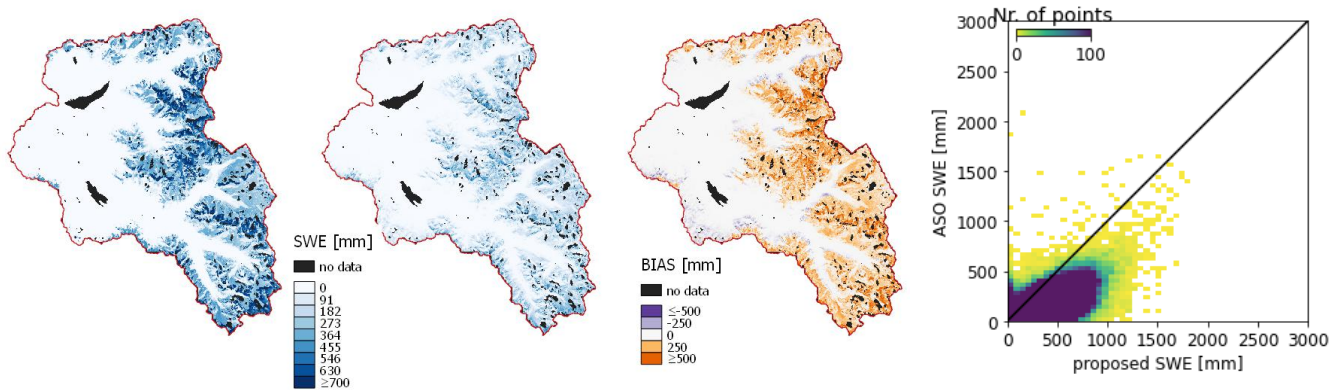
Figure S4. Proposed SWE (left), ASO SWE (centre-left), bias (centre-right) and dispersion graph (right) for the 12 analyzed dates over the three hydrological seasons (2018-2021) for the SFSJR. (cont.)



(j) 26 February 2021.

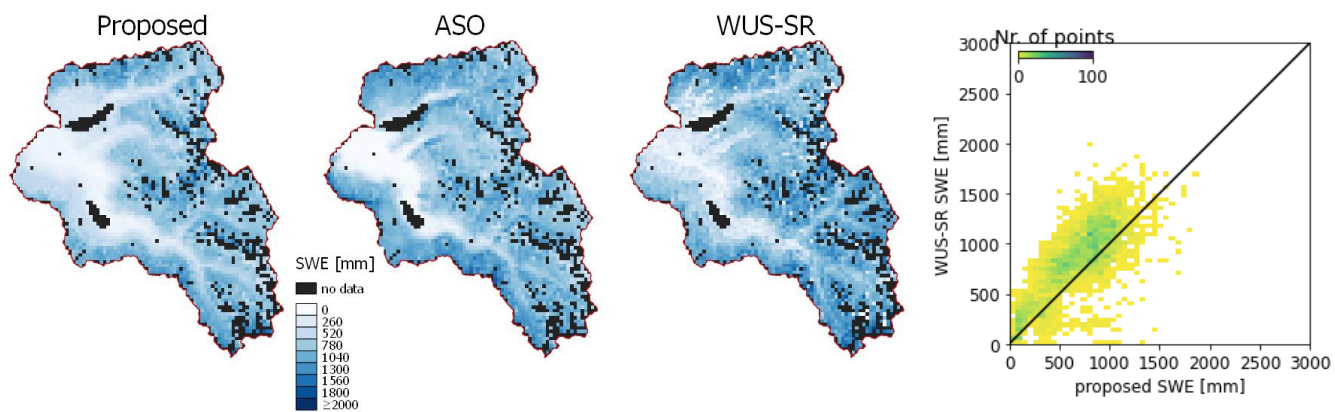


(k) 31 March 2021.

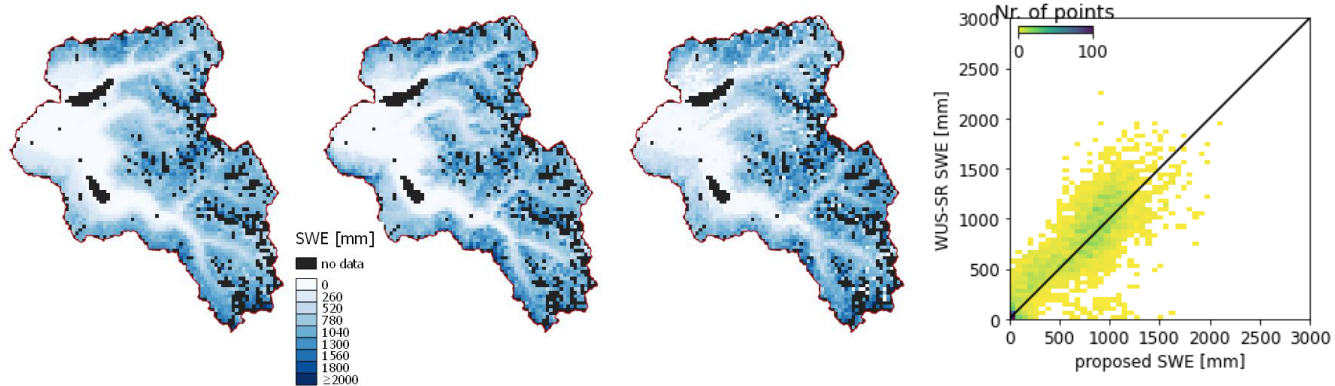


(l) 3 May 2021.

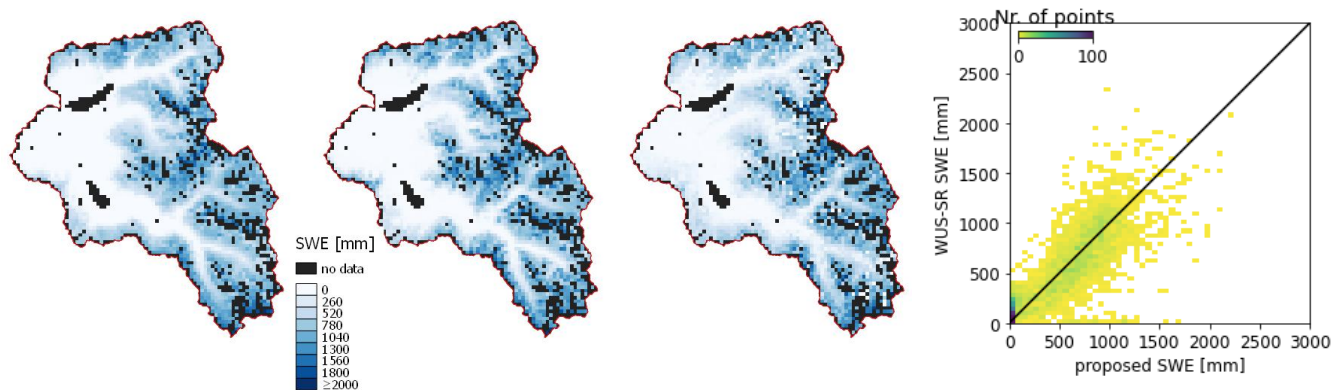
Figure S4. Proposed SWE (left), ASO SWE (centre-left), bias (centre-right) and dispersion graph (right) for the 12 analyzed dates over the three hydrological seasons (2018-2021) for the SFSJR. (cont.)



(a) 17 March 2019.

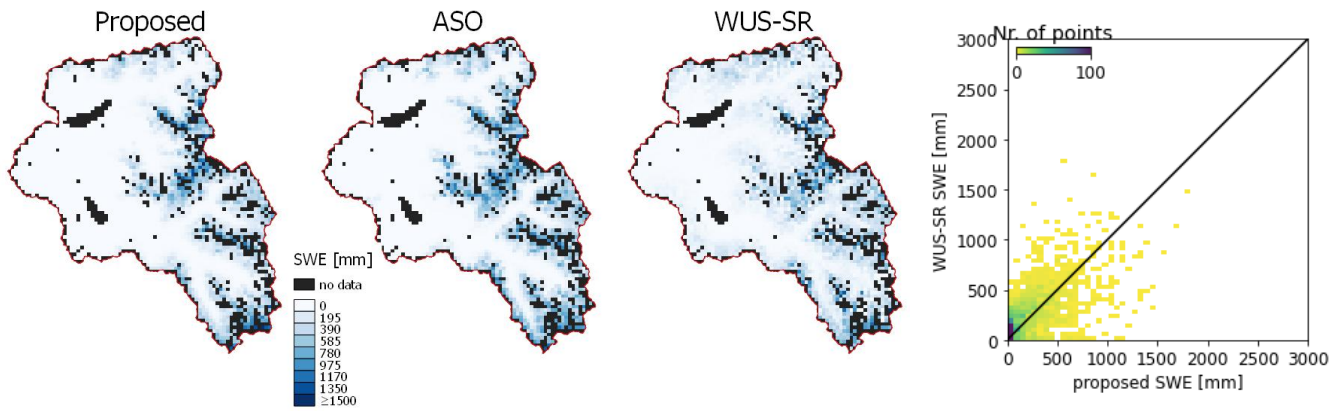


(b) 2 May 2019.

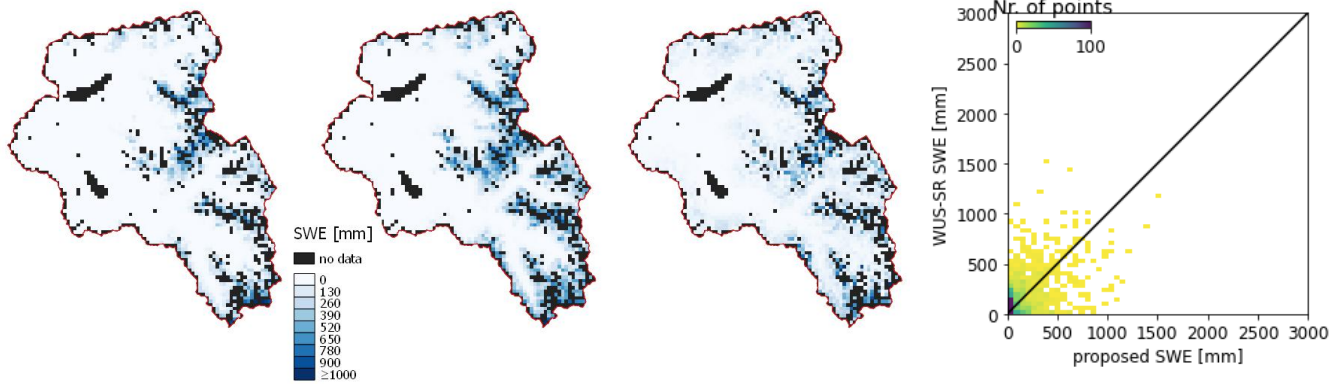


(c) 9 June 2019.

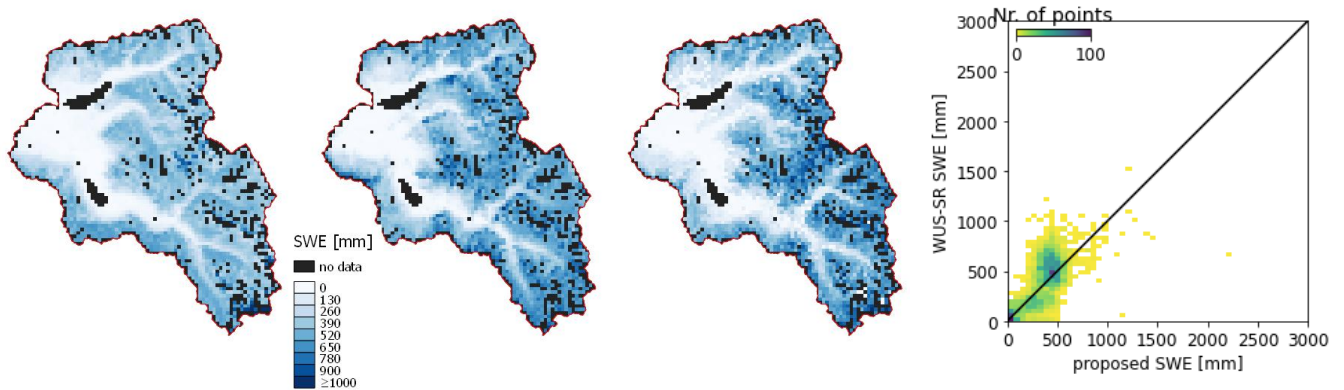
Figure S5. Proposed SWE (left), ASO SWE (centre-left), WUS-SR SWE (centre-right) and dispersion graph (right) for the 12 analyzed dates over the three hydrological seasons (2018-2021) for the SFSJR.



(d) 4 July 2019.

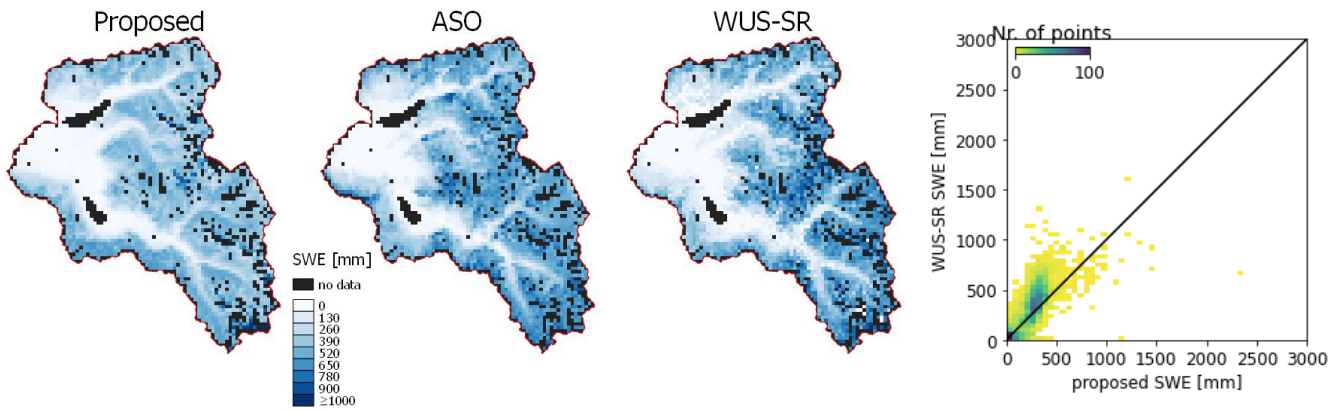


(e) 14 July 2019.

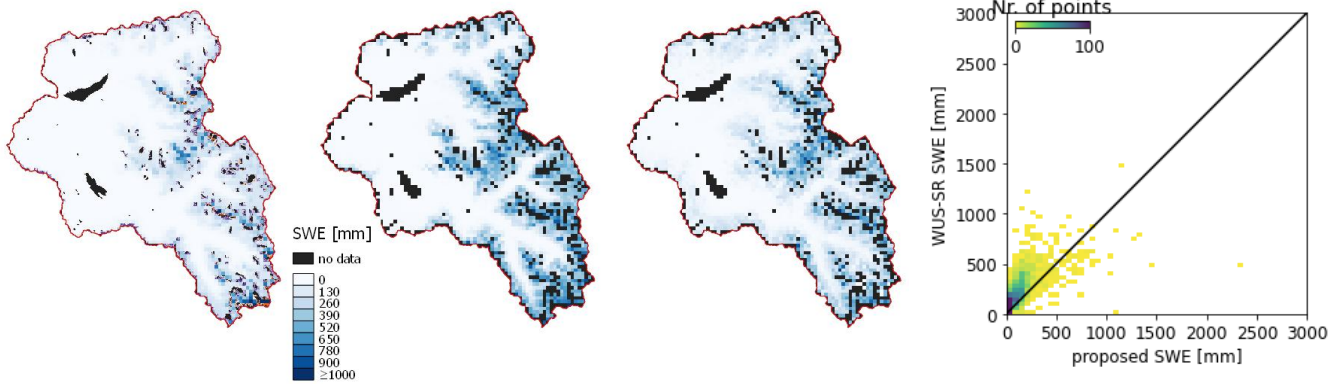


(f) 15 April 2020.

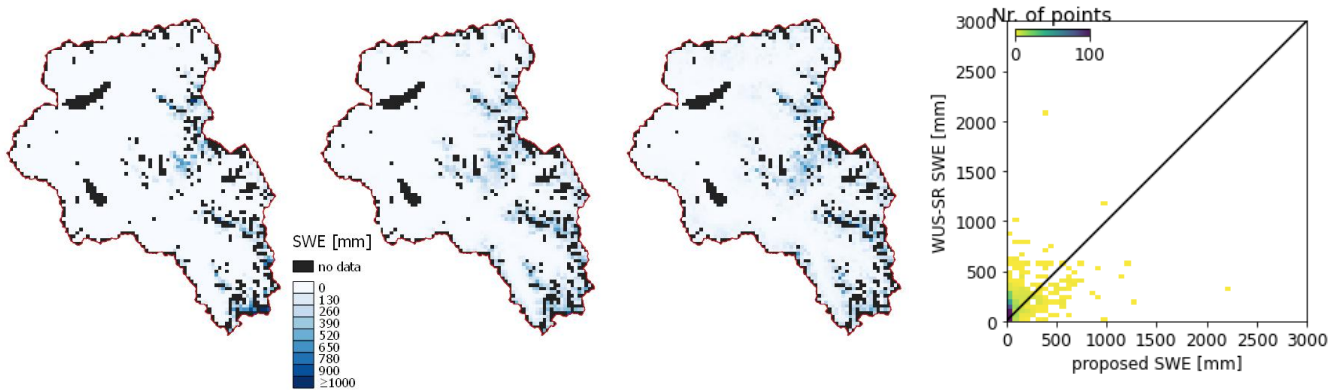
Figure S5. Proposed SWE (left), ASO SWE (centre-left), bias (centre-right) and dispersion graph (right) for the 12 analyzed dates over the three hydrological seasons (2018–2021) for the SFSJR. (cont.)



(g) 5 May 2020.

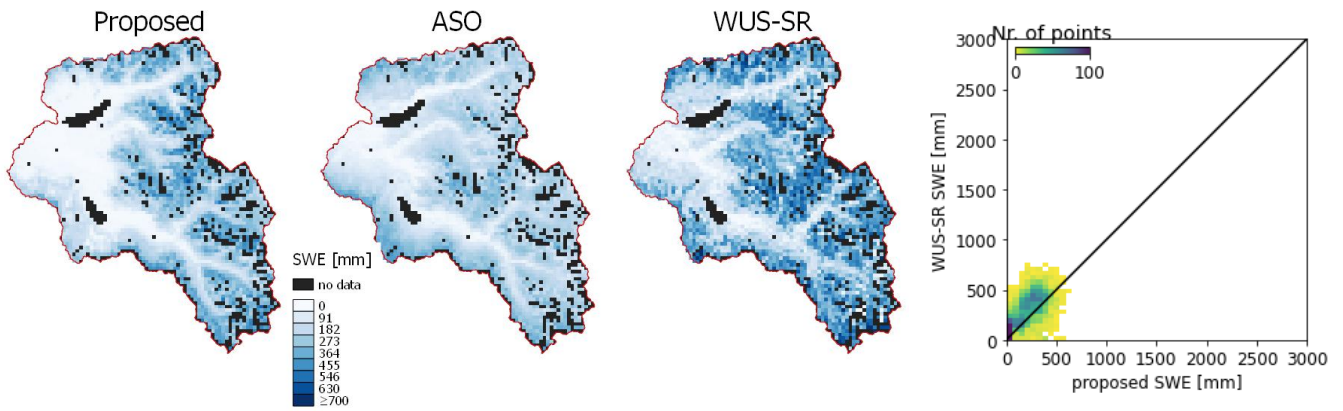


(h) 23 May 2020.

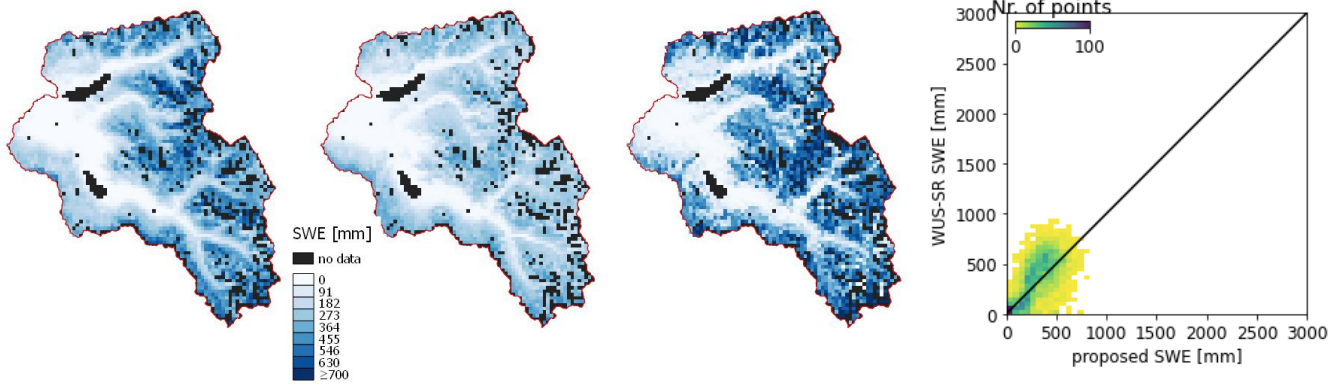


(i) 8 June 2020.

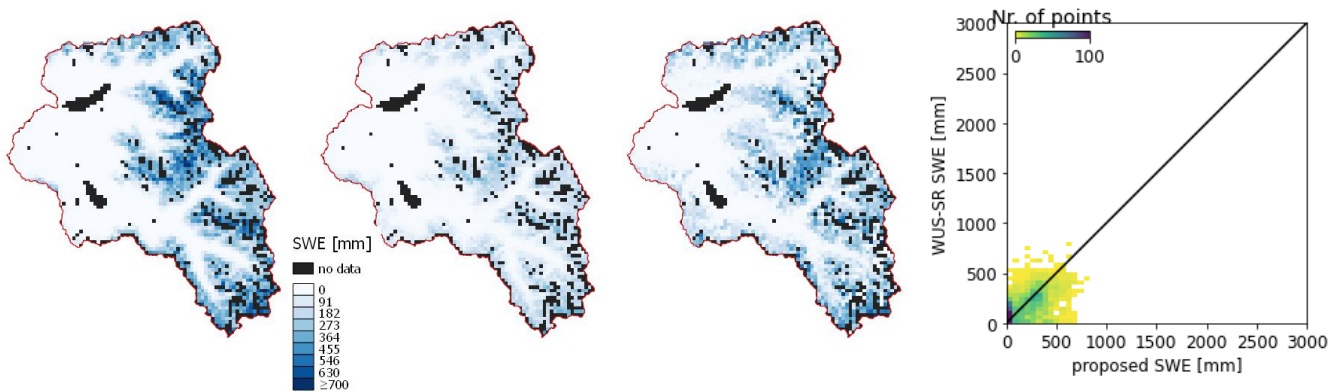
Figure S5. Proposed SWE (left), ASO SWE (centre-left), bias (centre-right) and dispersion graph (right) for the 12 analyzed dates over the three hydrological seasons (2018-2021) for the SFSJR. (cont.)



(j) 26 February 2021.

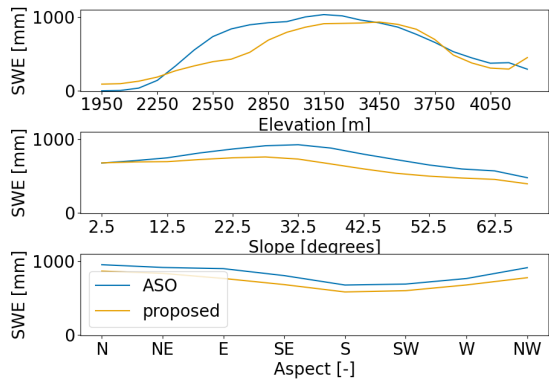


(k) 31 March 2021.

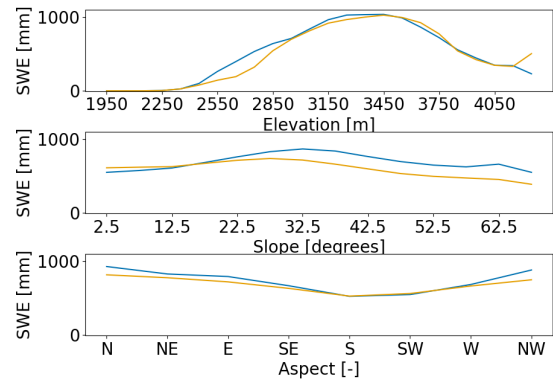


(l) 3 May 2021.

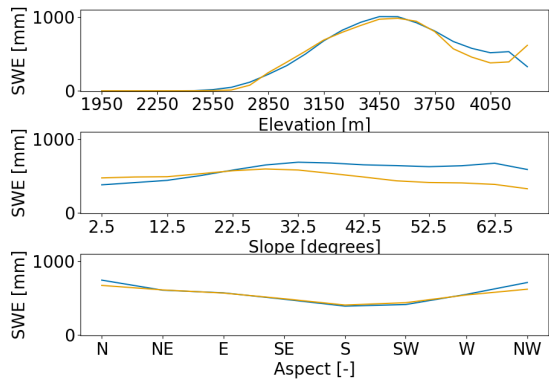
Figure S5. Proposed SWE (left), ASO SWE (centre-left), bias (centre-right) and dispersion graph (right) for the 12 analyzed dates over the three hydrological seasons (2018-2021) for the SFSJR. (cont.)



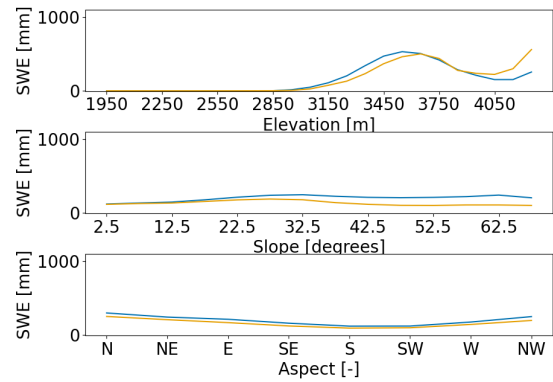
(a) 17 March 2019.



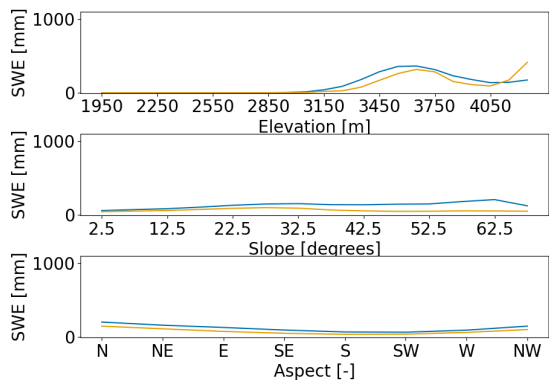
(b) 2 May 2019.



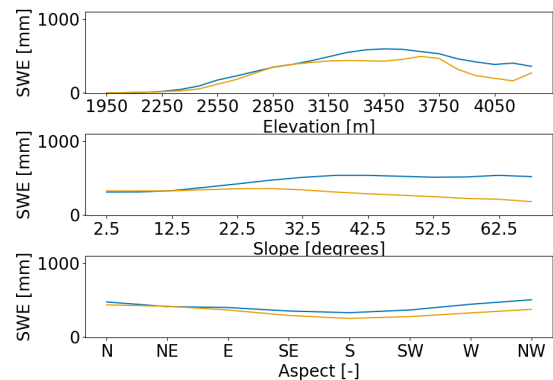
(c) 9 June 2019.



(d) 4 July 2019.

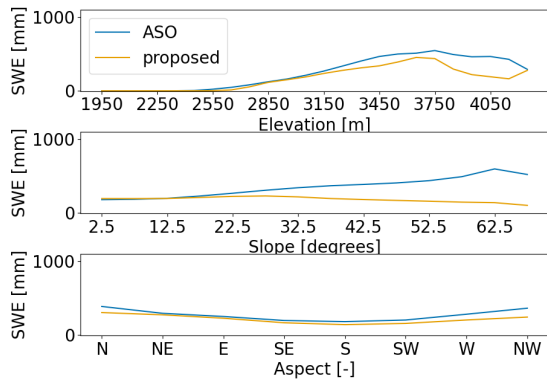


(e) 14 July 2019.

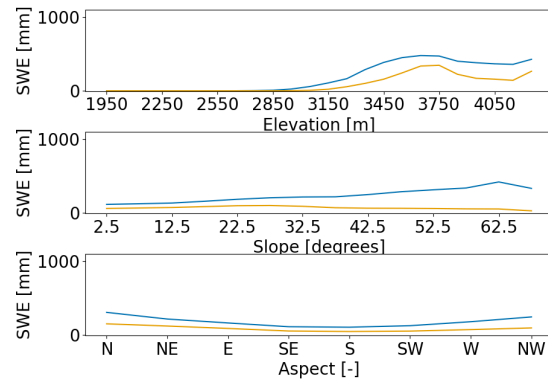


(f) 15 April 2020.

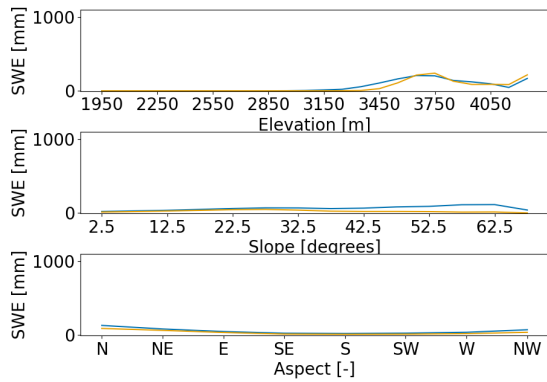
Figure S6. Mean SWE value for different elevation, slope and aspect belts. The proposed SWE dataset (in orange) is evaluated against ASO (in blue) for the 12 analyzed dates over the three hydrological seasons (2018-2021) for the SFSJR.



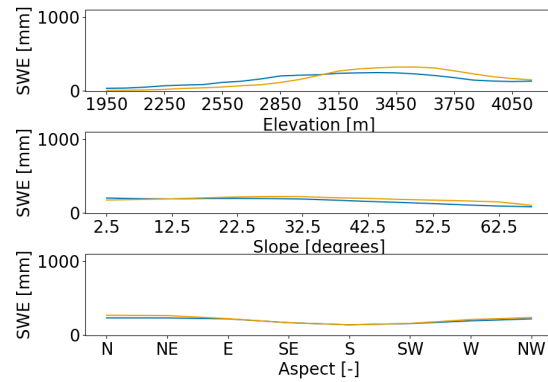
(g) 5 May 2020.



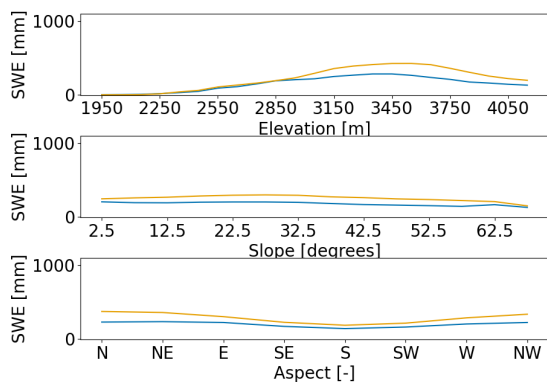
(h) 23 May 2020.



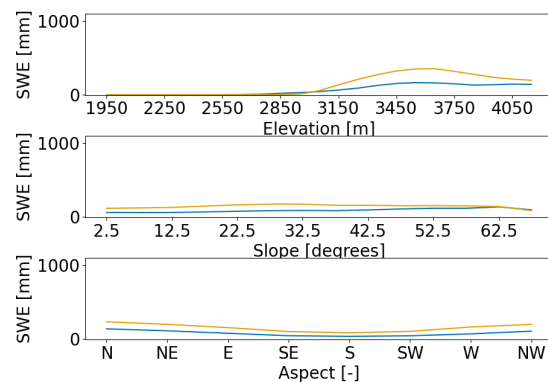
(i) 8 June 2020.



(j) 26 February 2021.



(k) 31 March 2021.



(l) 3 March 2021.

Figure S6. Mean SWE value for different elevation, slope and aspect belts. The proposed SWE dataset (in orange) is evaluated against ASO (in blue) for the 12 analyzed dates over the three hydrological seasons (2018-2021) for the SFSJR (cont.).

Table S1. Results of the intercomparison between the proposed SWE and the WUS-SR dataset versus ASO for the SFSJR. Bias, RMSE, and correlation are calculated pixel-wise. To this purpose, the proposed and ASO SWE maps were aggregated at a resolution of 500 m.

Date	BIAS [mm]		RMSE [mm]		Correlation [-]	
	proposed	WUS-SR	proposed	WUS-SR	proposed	WUS-SR
2019/03/17	-121	36	242	292	0.80	0.66
2019/05/02	-61	-4	208	307	0.90	0.77
2019/06/09	-25	-32	182	302	0.93	0.79
2019/07/04	-49	-14	129	201	0.90	0.71
2019/07/14	-51	-20	125	163	0.84	0.65
2020/04/15	-73	-26	159	169	0.80	0.78
2020/05/05	-59	5	151	154	0.82	0.80
2020/05/23	-95	-27	179	150	0.79	0.78
2020/06/08	-25	3	96	100	0.72	0.70
2021/02/26	5	96	92	157	0.75	0.65
2021/03/31	74	119	124	202	0.85	0.72
2021/05/03	65	54	121	121	0.89	0.66